Multilevel quantum beats: An analytical approach

C. Leichtle, I. Sh. Averbukh,* and W. P. Schleich†
Abteilung für Quantenphysik, Universität Ulm, D-89069 Ulm, Germany
(Received 30 July 1996)

We study the temporal behavior of generic transient signals originating from multilevel quantum systems. Such signals typically arise in the physics of wave packets in atoms, molecules, cavity QED, and ion traps and consist of a sum of a large number of harmonics whose frequencies depend nonlinearly on the sequential number of the harmonic. In particular, we focus on the semiclassical limit. Here, quantum beats between individual terms in the underlying sum lead to characteristic features of the signal in different time regimes, such as collapse, fractional revivals, and full revivals. We present a universal recipe for describing *analytically* all of the details of these features. Our approach is based on a specific representation of the sum of harmonics, which is most convenient in each of these time regions of interest. This brings out in a most natural way the phenomenon of fractional revivals and full revivals and explains their fine structures observed in recent experiments. [S1050-2947(96)01512-0]

PACS number(s): 42.50.Md, 32.90.+a

I. INTRODUCTION

Ultrashort laser pulses have opened a new and fascinating research area—the physics of atomic and molecular wave packets. Short pulses not only allow the excitation of a coherent superposition of many quantum states, but they also provide a tool to monitor its subsequent dynamics [1]. Being highly localized and hence particlelike objects, wave packets enable us to explore the quantum-classical border, and to touch such fundamental aspects of quantum mechanics as the correspondence principle [2]. On the other hand, the physics of wave packets is closely related to a practical field of laser femtochemistry, which studies molecular dynamics and chemical reactions ''in real time.'' Complicated time-resolved signals from packetlike excitations provide valuable information about the molecular energy spectrum and the shape of molecular potential surfaces [3,4].

Similar time-dependent signals originating from a large number of simultaneously excited quantum levels were recently studied in the context of atomic [5–19] and molecular [20–24] wave packets, cavity QED [25–35], and atom optics [36,37], only to mention a few. Despite the different physical nature of these systems and the studied signals, there is a surprising similarity in the overall structure of the temporal behavior of these signals.

In Figs. 1 and 2 we present two typical examples for such time-dependent quantities. Figure 1 shows the time-resolved emission of an electronic Rydberg wave packet created by a short laser pulse [5]. Figure 2 presents the calculated autocorrelation function $\mathcal{C}(t)=|\langle\psi(0)|\psi(t)\rangle|$ for a vibrational wave packet propagating in the excited potential surface $A^1\Sigma_u^+$ of a sodium dimer. Although the physical nature of the two systems as well as the displayed observables are rather different, both graphs show some surprising similarities. Initially, both pictures exhibit a sequence of regular peaks. The period T_1 of this pattern corresponds to the typical energy separation between neighboring excited levels. After some periods this behavior gradually disappears. However, the initial pattern recurs after a time T_2, which is much longer than T_1. For this reason this time scale T_2 is usually referred to [5] as the *revival time* [38].

For the electronic Rydberg wave packet in Fig. 1, T_2 is given by 5.2 ns, whereas for the nuclear wave packet of Fig. 2 one finds $T_2=94$ ps [39]. Moreover, these graphs also show that at *fractions* of this revival time again a periodic structure called *fractional revivals* [40] emerges, however now with a period, which is a *fraction* of T_1. The occurrence of full revivals and fractional revivals was observed in a number of experiments in atomic [14–19] and molecular

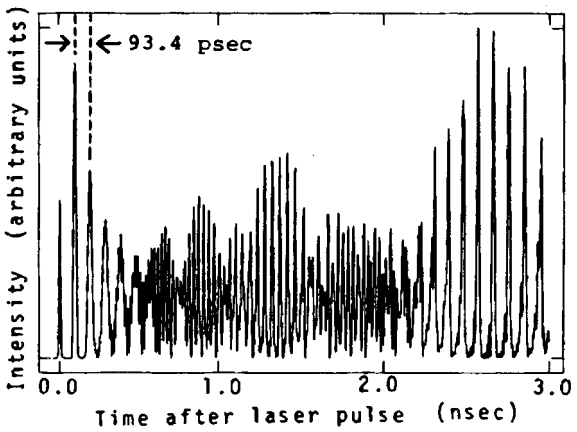

FIG. 1. Dynamics of an electronic wave packet monitored by the time-resolved intensity of spontaneous emission [5]. The wave packet was created by a short laser pulse resonant to a manifold of closely lying Rydberg states in hydrogen centered about the principal quantum number $\bar{n}=85$. Here, the initial beat pattern with period $T_1=93.4$ ps repeats itself after approximately $t\simeq 2.6$ ns. For further details, in particular for the method of calculating this signal, we refer to Ref. [5].

*Also Weizmann Institute of Science, Rehovot, 76100, Israel.

†Also Max-Planck-Institut für Quantenoptik, D-85748 Garching, Germany.

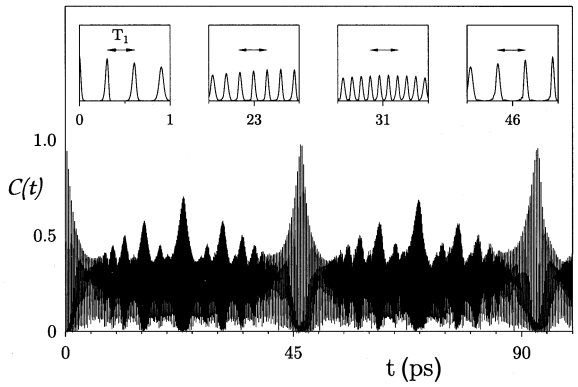

FIG. 2. Dynamics of a vibrational wave packet propagating in the excited electronic potential $A^1\Sigma_u^+$ in a sodium dimer. We show the autocorrelation function $\mathcal{C}(t)\equiv|\langle\psi(0)|\psi(t)\rangle|$, where the initial state $|\psi(0)\rangle$ is a replica of the ground state of the lower potential $X^1\Sigma_g^+$. This state may be created by a short laser pulse via a vertical electronic transition, and consists of several vibrational states of the potential $A^1\Sigma_u^+$. For this system the initial periodicity of $T_1=300$ fs shown in the inset in the left upper corner of the figure repeats itself after approximately 46 ps as shown by the inset in the upper right corner. The other insets which magnify the behavior of $\mathcal{C}(t)$ over a time duration of 1 ps around $t=23$ ps and $t=31$ ps reveal periods different from T_1. To bring this out most clearly we indicate the period T_1 by the arrow.

[23,24] systems. On the other hand, these phenomena have also attracted a lot of theoretical attention, e.g., in the context of atomic physics [5–13], molecular physics [20–22], quantum optics [25–31,34], and atom optics [36,37].

In the present paper we study such multilevel transient signals from a very general point of view. For time intervals, in which relaxation is still negligible, we present these signals in the most general form as

$$\mathcal{S}(t)=\sum_n P_n e^{i\omega(n)t}, \tag{1.1}$$

where $\omega(n)$ denotes the frequency of the harmonic with the sequential number n. The universal features of such transient signals are almost independent of the details of the weights P_n and the absolute sizes of the frequencies $\omega(n)$. Therefore we do not specify the physical meaning of these quantities, but only assume rather general properties such as smoothness, normalizability, etc.

Starting from Eq. (1.1), we present an analytical approach towards the typical features of transient signals, such as quasiperiodical behavior, dephasing, fractional revivals, and full revivals. All these physical phenomena are a result of quantum beats, which represent interference effects between *many* contributing terms in Eq. (1.1). However, due to this very reason it is hard to recognize the fine structure of the signal from the representation of $\mathcal{S}$ given in Eq. (1.1). In this paper we present a method to find closed-form expressions in distinguished time intervals of interest. These expressions depend only on general parameters determined by the system and the time interval under consideration. For this reason our approach allows us—despite its generality—to understand even quantitatively all the fine details of experimentally measured transient signals. As an example we explain the occurrence of oscillatory structures in the shape of fractional revivals observed experimentally in Rydberg wave packets [17].

The article is organized as follows. In Sec. II we cast the sum Eq. (1.1) into a form which reveals the different time regimes of the temporal behavior of $\mathcal{S}(t)$. In Sec. III we present a method convenient for analyzing the signal at the initial stage of the evolution by using the Poisson summation formula. With the help of this transformation we obtain a new representation of the sum $\mathcal{S}$, which brings out most clearly its features in this time regime. We generalize this method in Sec. IV to the description of fractional revivals and full revivals: We decompose the sum into subsums in a way which allows us to apply the same technique used in the analysis of the early stage of the evolution. Sections V and VI are devoted to the discussion of fractional revivals and full revivals with the help of this new representation. We finally summarize the main results of the paper in Sec. VII.

II. NATURAL TIME SCALES OF THE DYNAMICS

In the present section we rewrite the signal $\mathcal{S}(t)$, Eq. (1.1), so as to bring out the different time scales in its evolution. For the remainder of the paper we assume that the normalized distribution of weight factors P_n has a dominant maximum at the integer $\overline{n}\gg 1$ and a width Δn such that $\overline{n}\gg\Delta n\gg 1$. In this large n regime, that is, the semiclassical regime, the frequencies $\omega(n)$ of a physical system depend smoothly on the index n. This allows us to expand $\omega(n)$ in a Taylor series

$$\omega(n)=\omega(\overline{n})+\left.\frac{d\omega(n)}{dn}\right|_{n=\overline{n}}(n-\overline{n})+\frac{1}{2}\left.\frac{d^2\omega(n)}{dn^2}\right|_{n=\overline{n}}(n-\overline{n})^2+\frac{1}{6}\left.\frac{d^3\omega(n)}{dn^3}\right|_{n=\overline{n}}(n-\overline{n})^3+\cdots \tag{2.1}$$

around $\overline{n}$, which we write as

$$\omega(n)=\omega(\overline{n})+\sigma_1\frac{2\pi}{T_1}(n-\overline{n})+\sigma_2\frac{2\pi}{T_2}(n-\overline{n})^2+\sigma_3\frac{2\pi}{T_3}(n-\overline{n})^3+\cdots. \tag{2.2}$$

Here, we have defined $2\pi/T_j\equiv(j!)^{-1}|\omega^{(j)}(\overline{n})|$, and $\sigma_j=\pm 1$ accounts for the sign of the jth derivative $\omega^{(j)}(\overline{n})\equiv d^j\omega/dn^j|_{n=\overline{n}}$. Note that the value of σ_1 can always be assumed to be $+1$, since the energy of a bound state of a quantum system increases with the quantum number n.

When we insert Eq. (2.2) into Eq. (1.1) we find

$$\mathcal{S}(t)=\exp[i\omega(\overline{n})t]S(t), \tag{2.3}$$

where

$$S(t)=\sum_{m=-\infty}^{\infty} P_{\overline{n}+m}\exp\left[2\pi i\left(\frac{t}{T_1}m+\sigma_2\frac{t}{T_2}m^2+\sigma_3\frac{t}{T_3}m^3+\cdots\right)\right]. \tag{2.4}$$

Here, we have introduced the summation index $m=n-\overline{n}$. It is the sum $S(t)$, Eq. (2.4), which we analyze in the remainder of this article.

We gain deeper insight into the expansion Eq. (2.1) of ω with respect to n and into the time scales T_j when we recall that in the semiclassical limit the action J is proportional to the quantum number n of the bound state. With $J=n\hbar$ and $E=\hbar\omega=H$, where H denotes the Hamiltonian, we therefore arrive at

$$\frac{\partial\omega}{\partial n}=\frac{\partial(\hbar\omega)}{\partial(\hbar n)}=\frac{\partial H}{\partial J}. \tag{2.5}$$

This relation allows us to express the derivatives $\omega^{(j)}$ of the frequency ω with respect to n in terms of derivatives of the Hamiltonian and Planck's constant $\hbar$. Indeed, we find using $J=n\hbar$ the relation

$$\frac{\partial^j\omega}{\partial n^j}=\frac{\partial^{j-1}}{\partial n^{j-1}}\frac{\partial H}{\partial J}=\hbar^{j-1}\frac{\partial^j H}{\partial J^j}. \tag{2.6}$$

Hence the expansion (2.1) of ω corresponds to an expansion in powers of $\hbar$. Since the times T_j are the inverse of the derivatives $\omega^{(j)}$, they are proportional to the inverse powers $\hbar^{-j+1}$ and therefore satisfy the hierarchy

$$T_1\ll T_2\ll T_3\ll\cdots. \tag{2.7}$$

To illustrate the typical temporal behavior of a sum of the form Eq. (2.4), we use the specific example of a Gaussian distribution [41]

$$P_n=\frac{1}{\sqrt{2\pi\Delta n^2}}\exp\left[-\frac{(n-\overline{n})^2}{2\Delta n^2}\right], \tag{2.8}$$

with the variance $\Delta n=8$. Note that due to the shift in the summation over $m=n-\overline{n}$, Eq. (2.4), the parameter $\overline{n}$ only enters into the times T_j. In the present example we do not specify the functional dependence of $\omega(n)$ on n but choose $T_2=160T_1$ and $T_3=1000T_2$. Moreover, we set all higher time scales in the expansion in Eq. (2.2) equal to infinity. Hence in this way $\overline{n}$ does not enter explicitly. In addition we have taken $\sigma_2=\sigma_3=1$.

In Fig. 3 we show the overall structure of the sum $|S(t)|$ over a long-time interval. Here and in all of the following figures time is scaled in units of T_1. This graph reveals a complicated temporal dependence of $|S(t)|$ similar to the quantities displayed in Figs. 1 and 2.

Figures 4 and 5 magnify specific time intervals of Fig. 3 in order to resolve the fine structure of the signal. Figure 4 presents the early stage of the evolution: After a rapid decay shown in the inset we find in the beginning a periodic sequence of symmetric peaks separated by a period of T_1. However, in the course of time the peaks become broader until they overlap and form a complicated beat pattern. In our example, this happens approximately after three periods. Later on, as soon as the beats set in, we find fractional revivals [40] of various order, which follow each other very closely.

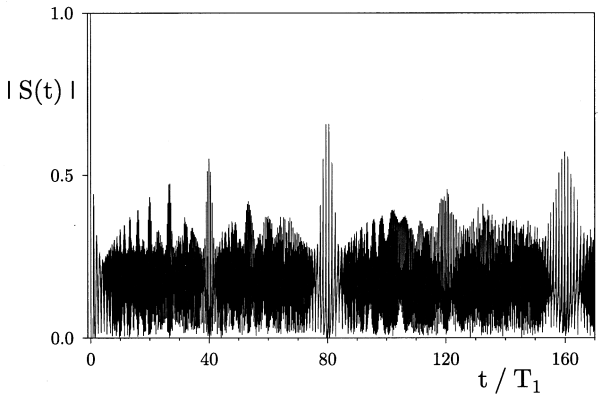

FIG. 3. Generic signal represented here by the time dependence of the sum $|S(t)|$, Eq. (2.4), for the case of a Gaussian distribution P_n with variance $\Delta n=8$. We have chosen the parameters $T_2=160T_1$ and $T_3=1000T_2$ with $\sigma_1=\sigma_2=\sigma_3=1$ and have set all higher time scales in Eq. (2.2) equal to infinity. The sum reveals a fairly complicated temporal behavior.

In Fig. 5 we present magnified sections of Fig. 3 in the vicinity of the times $t=\frac{1}{4}T_2=40T_1$ (a), $t=\frac{1}{3}T_2=53.33T_1$ (b), $t=\frac{1}{2}T_2=80T_1$ (c), and $t=T_2=160T_1$ (d), respectively. We recognize the following characteristic features: The sum S again involves periodic sequences of peaks; however, now the period between two neighboring peaks is given by $T_1/2$, $T_1/3$, T_1, as well as T_1, respectively. Figures 5(a)–5(c) show fractional revivals whereas Fig. 5(d) depicts a full revival. The larger the time $t=(1/r)T_2$ (here $r=4,3,2,1$), the larger the difference of the fine structure compared to the symmetric peaks in the initial stage of the evolution. Especially, for larger times the fractional revivals become more

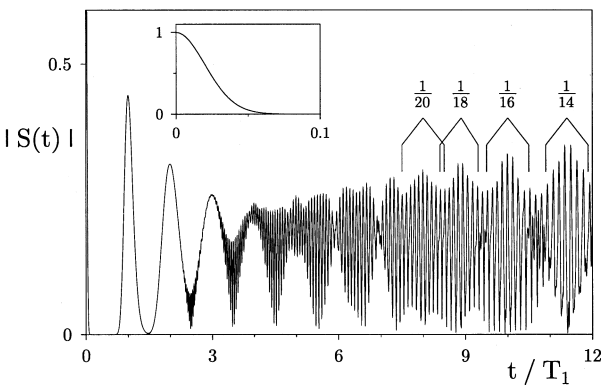

FIG. 4. Generic signal of Fig. 3 in its early stage, that is, for times up to $t=12T_1$. After a rapid decay magnified in the inset we note symmetric peaks with period T_1 which broaden and decay in height. At around $t\cong 3T_1$ rapid oscillations set in and a complicated beat structure develops. Note that as soon as this pattern emerges, we find fractional revivals of various orders. In the vicinity of $t=\frac{1}{20}T_2=8T_1$ we find ten peaks within a period of T_1, whereas in the vicinities of $t=\frac{1}{18}T_2=8.9T_1$, $t=\frac{1}{16}T_2=10T_1$, and $t=\frac{1}{14}T_2=11.4T_1$ we find nine, eight, and seven peaks within a period of T_1, respectively.

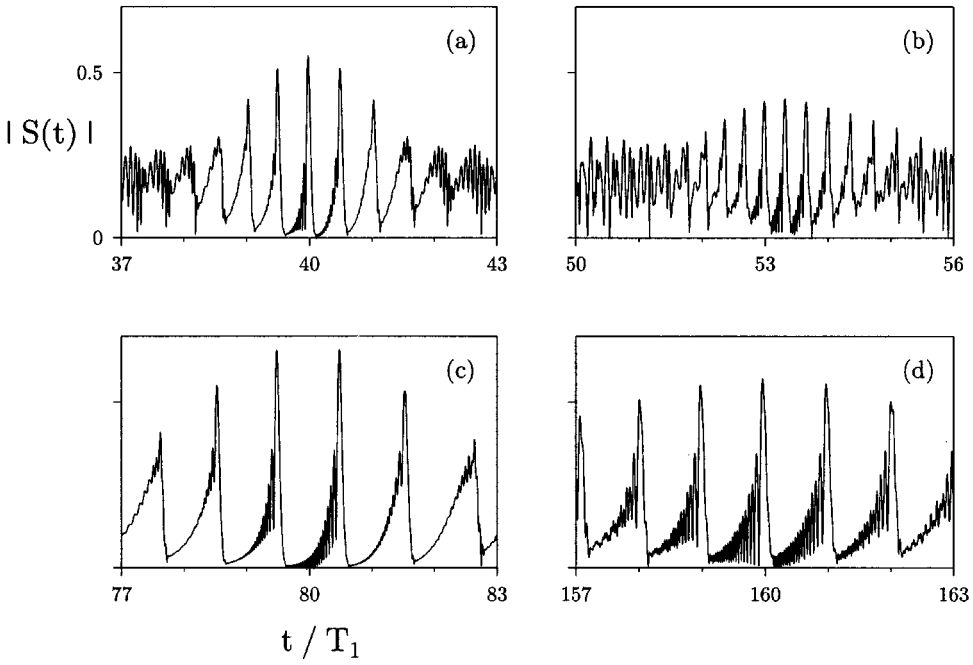

FIG. 5. Generic signal of Fig. 3 at later times. Here we magnify the behavior of $|S(t)|$ for time intervals of length $6T_1$ around distinguished times. The cases (a) and (b) show fractional revivals in the vicinity of $t=\frac{1}{4}T_2=40T_1$ and $t=\frac{1}{3}T_2=53.33T_1$, respectively. Note that the period of the fractional revivals in (a) is given by $T_1/2$ and in (b) by $T_1/3$. A complicated beat pattern arises as soon as neighboring peaks start to overlap considerably as exemplified by the behavior of $|S(t)|$ at the edges of (a) and (b). Moreover, we recognize that the shape of the peaks becomes asymmetric, and oscillations appear on the left hand side of the maximum. The cases (c) and (d) focus on fractional revivals in the vicinity of $t=\frac{1}{2}T_2=80T_1$, and on the full revivals in the vicinity of $t=T_2=160T_1$. The period of the fractional revivals in (c) as well as of the full revivals in (d) is given by T_1. However, the fractional revivals are shifted by half of the period T_1. Moreover, the shapes of the fractional revivals and the full revivals are highly asymmetric, that is, they show a slow oscillatory onset to the left of their maximum, and a rapid decay to the right. In all four cases the height of the peaks is controlled by a slowly varying envelope. The scales of the vertical axes are identical in all four examples.

and more asymmetric: They show an abrupt break-off on the right domain to their center, whereas on the left domain they decay much more slowly. Moreover, they show oscillations on top of this slow decay. Note that similar structures were found experimentally in the case of a Rydberg wave packet in rubidium [17]. We further notice that the heights of the fractional revivals seem to be modulated by a slowly varying amplitude with its center at the time point $t=(1/r)T_2$: As fractional revivals are located further away from this center, their dominant maximum decreases, the width broadens, and the small oscillations on the left to their center smear out.

This behavior is not obvious from the *form* of S in Eq. (2.4). In the next two sections we therefore cast the sum into a form which brings out in a clear way the period of the peaks and the fine details of their shape. In Sec. III we start with the analysis of the initial evolution and in Sec. IV we present our approach to analyzing the fine structure of fractional revivals and full revivals.

III. THE EARLY STAGE OF THE EVOLUTION

The phase factor of each term in Eq. (2.4) consists of the product of the factors $\exp(2\pi imt/T_1)$, $\exp(2\pi i\sigma_2 m^2 t/T_2)$, $\exp(2\pi i\sigma_3 m^3 t/T_3)$, etc. The relative importance of these factors depends strongly on the specific time under consideration. In the early stage of the evolution, that is, for times t of the order of T_1, the main contribution to the phase comes from the first factor $\exp(2\pi imt/T_1)$. Hence all the terms in the sum $S(t)$ are in phase for times t which are multiples of the period T_1. Therefore we expect a sequence of spikes in the signal located near the time points $t_l=lT_1$, where $l=1,2,\ldots$. However, as time increases, the second factor $\exp(2\pi i\sigma_2 m^2 t/T_2)$ also becomes important. Its contribution leads to a growing dephasing of neighboring terms in the sum Eq. (2.4) at the time points t_l, which results in a broadening of the spikes. This becomes apparent [42] when we rewrite the sum S with the help of the Poisson summation formula [43]

$$\sum_{m=-\infty}^{\infty} f_m = \sum_{l=-\infty}^{\infty} \int_{-\infty}^{\infty} dm f(m)\exp(-2\pi ilm), \quad (3.1)$$

which yields

$$S(t)=\sum_{l=-\infty}^{\infty} \int_{-\infty}^{\infty} dm P(\overline{n+m})\exp\left\{2\pi i\left[\left(\frac{t}{T_1}-l\right)m + \sigma_2\frac{t}{T_2}m^2+\sigma_3\frac{t}{T_3}m^3+\cdots\right]\right\}. \quad (3.2)$$

Here, $P(\overline{n+m})$ denotes the continuous version of the discrete distribution $P_{\overline{n+m}}$. We note that there are many con-

tinuous extensions of the discrete weights P_n. For the example of the Gaussian Eq. (2.8) we choose the extension

$$P(x)=\frac{1}{\sqrt{2\pi\Delta n^2}}\exp\left[-\frac{(x-\overline{n})^2}{2\Delta n^2}\right], \tag{3.3}$$

but emphasize that the treatment presented here is valid for an arbitrary weight distribution P_n.

What is the physical meaning of the transformation Eq. (3.1)? The Poisson summation formula allows us to represent a discrete superposition of many harmonics such as the sum S as a sequence of time-dependent signals numbered by the index l and arriving one after another. The application of this formula leads to a significant simplification when the width of each signal in time is shorter than the separation between two signals.

To bring this out most clearly we now consider times much smaller than $T_j/(\Delta n)^j$, where $j\geqslant 3$, and keep the first two terms in the exponent of Eq. (3.2) only. In this case, the integral for the Gaussian distribution Eq. (3.3) is of the form

$$\int_{-\infty}^{\infty} dx\ \exp(-ax^2+bx)=\sqrt{\frac{\pi}{a}}\exp\left(\frac{b^2}{4a}\right), \tag{3.4}$$

with

$$a\equiv\frac{1}{2\Delta n^2}-2\pi i\sigma_2\frac{t}{T_2} \tag{3.5}$$

and

$$b\equiv 2\pi i\left(\frac{t}{T_1}-l\right). \tag{3.6}$$

When we make use of this relation the sum S reads

$$S(t)\cong\sum_{l=-\infty}^{\infty}\frac{1}{\sqrt{1-i\sigma_2 4\pi\Delta n^2 t/T_2}} \times\exp\left[-\frac{2\pi^2\Delta n^2}{1-i\sigma_2 4\pi\Delta n^2 t/T_2}\left(\frac{t}{T_1}-l\right)^2\right]. \tag{3.7}$$

We separate the real and imaginary parts in the exponent and arrive at

$$S(t)\cong\sum_{l=-\infty}^{\infty}\frac{1}{\sqrt{1-i\sigma_2 4\pi\Delta n^2 t/T_2}}\exp\left[-\frac{(t-lT_1)^2}{2\sigma_r^2(t)}\right] \times\exp\left[-i\sigma_2\frac{(t-lT_1)^2}{2\sigma_i^2(t)}\right], \tag{3.8}$$

where the width

$$\sigma_r^2(t)\equiv\left[\frac{1}{4\pi^2\Delta n^2}+4\Delta n^2\left(\frac{t}{T_2}\right)^2\right]T_1^2 \tag{3.9}$$

and

$$\sigma_i^2(t)\equiv\left[\frac{1}{16\pi^3\Delta n^2 t/T_2}+\frac{1}{\pi}\Delta n^2\frac{t}{T_2}\right]T_1^2 \tag{3.10}$$

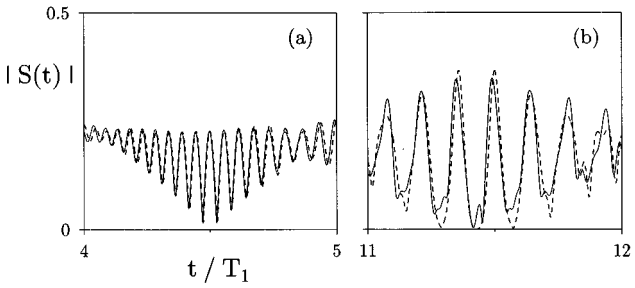

FIG. 6. Comparison between exact numerical evaluation of the generic signal $|S(t)|$, Eq. (2.4), (solid line) and the approximate expression Eq. (3.8) (dashed line) in the early stage of the evolution. Whereas for times shown in (a) the two curves are almost indistinguishable, they show deviations for larger times displayed in (b). In both cases the approximation works well for times at the center of each frame and gets worse towards the edges. The scales on the vertical axes in (a) and (b) are identical.

of the real and the imaginary Gaussians increase as a function of time.

Indeed, Eq. (3.8) gives the coherent signal $S(t)$ as a sequence of complex Gaussians centered at the time points $t_l=lT_1$. Two consecutive terms of the sum Eq. (3.8) separate in time, when their temporal separation $t_l-t_{l-1}=T_1$ is larger than their width $\delta t_l=2\sqrt{2}\sigma_r(t_l)$, that is, if $T_1>\delta t_l$. We illustrate this with the help of the previous example shown in Fig. 4. For the parameters used there, we estimate the first term in the brackets in Eq. (3.9) by $1/(4\pi^2\Delta n^2)\sim 4\times 10^{-4}$. The second contribution we estimate by $4\Delta n^2(t/T_2)^2\sim 4\Delta n^2(T_1/T_2)^2\sim 10^{-2}$. Hence we can neglect the first contribution compared to the second one and estimate the width δt_l of the lth Gaussian by

$$\delta t_l=2\sqrt{2}\sigma_r(t_l=lT_1)\cong 4\sqrt{2}\Delta n l\frac{T_1}{T_2}T_1. \tag{3.11}$$

Hence the Gaussians overlap and interfere with each other when $4\sqrt{2}\Delta n l T_1/T_2\sim 1$ or $l\sim T_2/(4\sqrt{2}\Delta n T_1)$. In our example this corresponds to $l\sim 3.5$. This is in good agreement with Fig. 4, where indeed the complicated beat pattern starts after approximately $t=3.5T_1$.

In Fig. 6 we compare by a dashed line the approximation Eq. (3.8) to the exact curve shown by the solid line. Whereas initially in (a) a difference between the exact sum and expression Eq. (3.8) can hardly be recognized, the approximation, which neglected the cubic term in the exponent, becomes worse for longer times as shown in (b).

IV. A NEW REPRESENTATION OF THE SUM

We now turn to larger times for which the phase difference between two consecutive terms at the time points t_l in the sum Eq. (2.4) is not close to an integer multiple of 2π. In this time regime the representations Eqs. (3.2) and (3.8) are inconvenient since the interference between neighboring signals is important. Indeed, it is the interference of the complex Gaussians in Eq. (3.8) which eventually leads to the formation of fractional revivals, as shown in Figs. 4 and 6 for times $t\sim 3T_1$ and larger. However, neither the period nor the shape of the fractional revivals can be seen from the form of

the sum S in Eq. (3.8). Thus in this time regime the representation Eq. (3.8) of the sum Eq. (1.1) is no longer useful. But can we cast the sum S Eq. (2.4) in a form which brings out the period and the shape of the fractional revivals and revivals?

The answer is yes. The key idea of our approach is a decomposition of the sum Eq. (2.4) into a number of subsums, each of which contains only terms whose phases are close to each other. We achieve this by combining each rth term of the original sum Eq. (2.4) to one subsum. The particular choice of r depends on the time interval under consideration.

Indeed, consider the behavior of S in the neighborhood of the time $t=(q/r)T_2$ of a fractional revival [40,49]. Here, q/r are mutually prime integers. It is of advantage to shift the origin of time into the region of $(q/r)T_2$ and choose it to be an integer multiple l of T_1, that is,

$$t \equiv lT_1 + \Delta t \equiv \frac{q}{r} T_2 + \epsilon_{q/r} T_1 + \Delta t. \tag{4.1}$$

Here, the absolute value of the remainder $\epsilon_{q/r} T_1 \equiv lT_1 - (q/r)T_2$ is less than or equal to half of the period T_1, that is, $|\epsilon_{q/r}| \leq 1/2$. This choice allows us to bring the sum S, Eq. (2.4), into the form

$$S(\Delta t) \equiv S\left(t = \frac{q}{r} T_2 + \epsilon_{q/r} T_1 + \Delta t \right) = \sum_{m=-\infty}^{\infty} \gamma_m^{(r)} W_m(\Delta t), \tag{4.2}$$

where

$$\gamma_m^{(r)} \equiv \exp\left(2\pi i \sigma_2 \frac{q}{r} m^2 \right) \tag{4.3}$$

and

$$W_m(\Delta t) \equiv P_{\overline{n+m}} \exp\left\{ 2\pi i \left[\frac{\Delta t}{T_1} m + \sigma_2 \left(\epsilon_{q/r} + \frac{\Delta t}{T_1} \right) \frac{T_1}{T_2} m^2 + \sigma_3 \left(l + \frac{\Delta t}{T_1} \right) \frac{T_1}{T_3} m^3 + \cdots \right] \right\}. \tag{4.4}$$

Here, we have used the relation $\exp(2\pi imt/T_1) = \exp(2\pi iml)\exp(2\pi im\Delta t/T_1) = \exp(2\pi im\Delta t/T_1)$. We note that this representation of the sum S depends on the choice of the origin of time and thus on the fraction q/r. Hence for every different time region under consideration we adopt a different representation of the sum S.

We proceed by noting that the function $\gamma_m^{(r)}$ Eq. (4.3) is periodic in m with period r, that is, $\gamma_{m+r}^{(r)} = \exp[2\pi i \sigma_2 q/r(m+r)^2] = \gamma_m^{(r)}$. This periodicity depends only on the denominator r of the fraction q/r. In order to make use of this periodicity we rearrange the summation with the help of the relation

$$\sum_{m=-\infty}^{\infty} a_m = \sum_{p=0}^{r-1} \sum_{k=-\infty}^{\infty} a_{p+kr}, \tag{4.5}$$

that is, we first sum the terms a_m at all multiples kr of this period r and then sum these subsums over one period [44]. Since $\gamma_{p+kr}^{(r)} = \gamma_p^{(r)}$ we find

$$S(\Delta t) = \sum_{p=0}^{r-1} \gamma_p^{(r)} \sum_{k=-\infty}^{\infty} W_{p+kr}(\Delta t). \tag{4.6}$$

For the subsum over the index k we now face the same situation as for the entire sum S Eq. (2.4) at the initial stage of the temporal evolution. We can therefore apply the Poisson summation formula Eq. (3.1) to the subsums over k which yields

$$S(\Delta t) = \sum_{p=0}^{r-1} \gamma_p^{(r)} \sum_{m=-\infty}^{\infty} \int_{-\infty}^{\infty} dk W(p+kr, \Delta t) \times \exp(-2\pi ikm), \tag{4.7}$$

where $W(x,\Delta t)$ is the continuous version of $W_m(\Delta t)$, Eq. (4.4). As discussed in Sec. III the Poisson summation formula allows us to represent each time-dependent subsum as a sequence of time-dependent signals numbered by the index m.

When we introduce the new integration variable $x = p + kr$, the integral over x is independent of p, that is,

$$S(\Delta t) = \frac{1}{r} \sum_{p=0}^{r-1} \gamma_p^{(r)} \sum_{m=-\infty}^{\infty} \exp\left(2\pi i \frac{p}{r} m \right) \times \int_{-\infty}^{\infty} dx W(x, \Delta t) \exp\left(-2\pi i \frac{m}{r} x \right). \tag{4.8}$$

We interchange the two summations and write the sum S in the form

$$S(\Delta t) = \sum_{m=-\infty}^{\infty} \mathcal{W}_m^{(r)} I_m^{(r)}(\Delta t), \tag{4.9}$$

where

$$\mathcal{W}_m^{(r)} = \frac{1}{r} \sum_{p=0}^{r-1} \exp\left[2\pi i \left(\sigma_2 p^2 \frac{q}{r} + p \frac{m}{r} \right) \right] \tag{4.10}$$

are time-independent coefficients and the factors

$$I_m^{(r)}(\Delta t) = \int_{-\infty}^{\infty} dx P(\overline{n+x}) \exp\left\{ 2\pi i \left[\left(\frac{\Delta t}{T_1} - \frac{m}{r} \right) x + \sigma_2 \left(\epsilon_{q/r} + \frac{\Delta t}{T_1} \right) \frac{T_1}{T_2} x^2 + \sigma_3 \left(l + \frac{\Delta t}{T_1} \right) \frac{T_1}{T_3} x^3 + \ldots \right] \right\} \tag{4.11}$$

represent the time-dependent signals.

Hence we have cast the infinite sum Eq. (2.4) into another infinite sum Eq. (4.9). The transformation of the sum, made possible by the shift of the origin of time as in Eq. (4.1), together with the decomposition of the sum into subsums as in Eq. (4.5) and the Poisson summation formula Eq. (3.1) is exact. But what is the advantage of this on-first-sight more

complicated representation of S? It reveals in the most obvious way the fractional revivals: Each term $I_m^{(r)}(\Delta t)$ is a fractional revival. However, in complete accordance with Sec. III this statement is correct, and hence the representation Eq. (4.9) is useful, only when the temporal width of the signal $I_m^{(r)}(\Delta t)$ is smaller than the separation between two neighboring signals.

V. CONSTITUENTS OF THE NEW REPRESENTATION

In the new representation Eq. (4.9), each term in the sum consists of the product of $\mathcal{W}_m^{(r)}$ and $I_m^{(r)}(\Delta t)$. We now discuss these constituents in more detail.

The factor $\mathcal{W}_m^{(r)}$ is independent of the distribution $P(n)$ and the time Δt. Thus it acts in the sum Eq. (4.9) as a weight. It is a well-known quantity in the context of fractional revivals [40]. According to Eq. (4.10), $\mathcal{W}_m^{(r)}$ is a sum of r complex numbers each with the modulus $1/r$. Hence the modulus of $\mathcal{W}_m^{(r)}$ ranges from zero to unity. The individual terms in the finite sum interfere and this interference depends on the parameters m and r via the phase angle $2\pi m/r$. Moreover, an additional r dependence enters via the phase $2\pi q/r$. Hence the value of $\mathcal{W}_m^{(r)}$ is on first sight a complicated function of m, r, and q. However, the detailed analysis of Ref. [40] reveals the following simple features: (i) For r even, $\mathcal{W}_m^{(r)}$ vanishes for every second value of m, whereas for r odd $\mathcal{W}_m^{(r)}$ is nonzero for every value of m, and (ii) the modulus $|\mathcal{W}_m^{(r)}|$ of each nonzero weighting factor is independent of q; in particular, one finds $|\mathcal{W}_m^{(r)}|=1/\sqrt{r}$ for r odd and $|\mathcal{W}_m^{(r)}|=\sqrt{2/r}$ for r even.

Now we turn to the discussion of the time-dependent term $I_m^{(r)}(\Delta t)$, which contains the information about the location, the duration, and the detailed shape of the signal. To be specific, we employ our previous example of a Gaussian distribution for the weight function $P(n)$. If higher order terms in the exponent in Eq. (4.11) indicated by the dots are still negligible, we again can evaluate the integral $I_m^{(r)}(\Delta t)$ analytically as shown in Appendix A, which yields

$$I_m^{(r)}(\Delta t)=\exp[i\Phi_m(\Delta t)]G(\Delta t)F_m(\Delta t)\mathrm{Ai}(z_m(\Delta t)). \tag{5.1}$$

Here, the functions $G(\Delta t)$ and $F_m(\Delta t)$ are defined by

$$G(\Delta t)\equiv A\exp\left[-\lambda\left(\epsilon_{q/r}+\frac{\Delta t}{T_1}\right)^2\right] \tag{5.2}$$

and

$$F_m(\Delta t)\equiv\exp\left[\mu\left(\frac{\Delta t}{T_1}-\frac{m}{r}\right)\right] \tag{5.3}$$

and $\mathrm{Ai}(z)$ denotes the Airy function of complex argument. The quantities Φ_m, A, λ, and μ are real whereas z_m is complex. In the neighborhood $|\Delta t|\sim T_1$ of a fractional revival time $t=(q/r)T_2$ the quantities A, λ, and μ can be considered as time independent whereas $\Phi_m(\Delta t)$ and $z_m(\Delta t)$ depend on Δt. For the definition of these quantities we refer to Appendix A.

According to Eq. (5.1) the time dependence of $I_m^{(r)}(\Delta t)$ is governed by the time dependence of the phase $\Phi_m(\Delta t)$, by the Gaussian $G(\Delta t)$, by the simple exponential $F_m(\Delta t)$, and an Airy function of complex argument. We now discuss the time dependence of each of these terms separately. For this purpose we use the specific fractional revival region in the vicinity of $t=\frac{1}{2}T_2=80T_1$ shown in Fig. 7(a). In this case the parameters l and $\epsilon_{1/2}$ take on the values $l=80$ and hence $\epsilon_{1/2}=0$, as can be found from Eq. (4.1).

We start our discussion with the Gaussian $G(\Delta t)$ shown in Figs. 7(b) and 7(c) by the dashed curve. Note that this function is independent of the summation index m. It is centered at $\Delta t=0$ and has the width $\delta t_G=2/\sqrt{\lambda}$, which equals $\delta t_G\simeq 3.8T_1$ for the example at hand. Next, we consider the exponential factor $F_m(\Delta t)$, which is equal to unity at the time point $\Delta t_m=(m/2)T_1$. Since in our case $\mu>0$ as shown in Eq. (A25), the exponential increases for increasing Δt as shown in the middle and the bottom of Fig. 7 by the dotted curve for the cases $m=1$ and $m=5$, respectively.

The Airy function of the complex-valued argument $z_m(\Delta t)$ requires more detailed considerations. Every value of m defines via Eq. (A21) a path $z_m(\Delta t)$ in the complex plane. Since in our example the weighting factor $\mathcal{W}_m^{(2)}$ vanishes for all even values of m as mentioned above, it is sufficient to restrict the discussion to odd values of m. In Fig. 8 we show the paths corresponding to $m=-7,-5,-3,-1,1,3,5,7$ for the time interval $-3T_1<\Delta t<3T_1$ of Fig. 7. For our parameters these paths are almost straight lines. We note from Eq. (A21) that only the real part of $z_m(\Delta t)$ depends on the index m and that this dependence is a linear one: Paths corresponding to different values of m are just shifted with respect to each other. This figure also includes by a dotted and a dashed line two of the anti-Stokes lines of the Airy differential equation defined [45] by $\arg(z)=\pm\pi/3$. Note that due to the different scales on the horizontal and the vertical axis these anti-Stokes lines appear as a single vertical line. Whenever a path traverses one of these anti-Stokes lines, the behavior of the Airy function changes drastically [45]: Whereas the Airy function decays exponentially in the domain on the right of the anti-Stokes lines, that is for $|\arg[z_m(\Delta t)]|<\pi/3$, it oscillates in the left domain, that is, for $|\arg[z_m(\Delta t)]|>\pi/3$. This behavior becomes immediately apparent when we recall the asymptotic behavior of the Airy function, which reads $\mathrm{Ai}(z)\sim\frac{1}{2}\pi^{-1/2}z^{-1/4}\exp(-\frac{2}{3}z^{3/2})$ for $z\to\infty$ and $|\arg(z)|<\pi$.

In order to study this behavior in more detail we show in Fig. 9 the absolute value of the complex Airy function as a rolling valley above the complex plane. For the analysis of fractional revivals in this time regime it is enough to understand the time dependence of the absolute value of the Airy function as we show in Sec. VI. In Fig. 9 we have also indicated by thick lines the paths $z_m(\Delta t)$ for $m=-5,-3,-1,1,3,5$ as well as two of the anti-Stokes lines in the complex plane. The thick lines running on the rolling valley display the value of $|\mathrm{Ai}(z)|$ along these paths z_m as well as along these anti-Stokes lines, that is, these lines depict $|\mathrm{Ai}(z_m(\Delta t))|$ and $|\mathrm{Ai}(z=|z|e^{\pm i\pi/3})|$, respectively. We recognize that indeed the Airy function oscillates in the do-

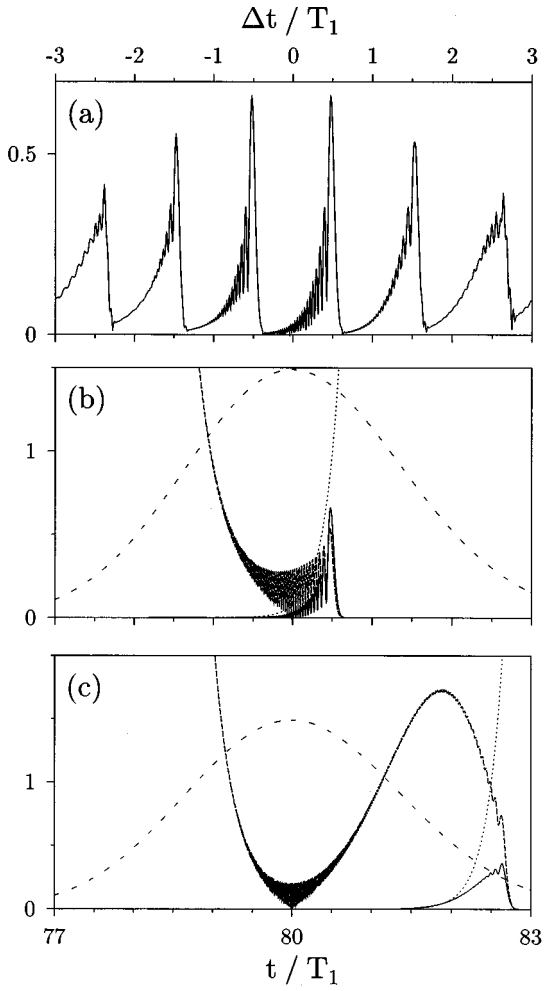

FIG. 7. Fractional revivals described by a single term in the new representation Eq. (4.9) of the generic signal $|S(t)|$. In (a) we repeat Fig. 5(c) and show the signal in the neighborhood of $t=\frac{1}{2}T_2=80T_1$. Moreover, we indicate on the top of the figure the relative time Δt introduced in Eq. (4.1). In (b) and (c) we show the terms $|I^{(2)}_{m=1}(\Delta t)|$ and $|I^{(2)}_{m=5}(\Delta t)|$, Eq. (5.1), of the new representation Eq. (4.9) of the sum $|S(\Delta t)|$ by a solid line. The individual contributions due to the Gaussian $G(\Delta t)$, Eq. (5.2), the exponential $F_m(\Delta t)$, Eq. (5.3), and the absolute value $|\mathrm{Ai}(z_m(\Delta t))|$ of the complex-valued Airy function are depicted by the dashed, dotted, and broken lines, respectively. Note that the scales of the vertical axes are different in all three cases. Whereas the exponential decays to the left and increases to the right of $\Delta t_{m=1}=\frac{1}{2}T_1=0.5T_1$ as shown in (b), the reverse is true for the Airy function. Hence it is the product of these two functions, which yields the pronounced peak of $|I^{(2)}_{m=1}(\Delta t)|$ centered at $\Delta t=0.5T_1$. The Gaussian, which is centered at $\Delta t=0$, just influences the height of this peak, since this function varies very slowly compared to the other two functions. Note that the fine structure of the peak results exclusively from the Airy function: Since in the vicinity of $\Delta t_{m=1}=0.5T_1$ the path z_1 runs very close to the real axis, as can be seen from Figs. 8 and 9, the absolute value of the Airy function of the complex argument $z_1(\Delta t)$ is almost identical to an Airy function of real argument. Hence the oscillations of the peak on top of the slow decay to the left of $\Delta t=0.5T_1$ are very deep and almost reach zero. In (c) it is again the product of the Airy function and the exponential which yields the peak of $|I^{(2)}_{m=5}(\Delta t)|$ centered now at $\Delta t_{m=5}=\frac{5}{2}T_1$. However, since the path z_5 contains a significant imaginary part as seen in Figs. 8 and 9, the Airy function exhibits only small oscillations around $\Delta t=2.5T_1$. Therefore the oscillations on top of the slow decay to the left of the peak are not as pronounced as in (b). The Gaussian is the overall envelope of this structure as already alluded to in Fig. 5.

main left of these anti-Stokes lines, whereas it decays rapidly in the domain right of these anti-Stokes lines. Note also the strong sensitivity of this function to the imaginary part of its argument. When we increase the absolute value of the imaginary part the oscillation amplitude decreases and the function increases. In Figs. 7(b) and 7(c) we show by a broken line the third factor of $|I^{(2)}_1|$ and $|I^{(2)}_5|$, that is, the values of $|\mathrm{Ai}(z_m)|$ along the paths $z_{m=1}$ and $z_{m=5}$, respectively.

Each crossing of an anti-Stokes line $\arg(z)=\pm\pi/3$ implies the end of the time-dependent signal $I^{(r)}_m(\Delta t)$. To find this moment we calculate in Appendix B the time $\Delta t^{(a)}_m$ at which the path $z_m(\Delta t)$ traverses an anti-Stokes line. We show that for our parameters and values of $|m|$ of the order of unity, this happens in the immediate vicinity of $\Delta t_m=(m/2)T_1$ where the exponential function F_m assumes the value of unity, that is, $\Delta t^{(a)}_m\cong\Delta t_m$. Since we are interested in the time interval $-3T_1\leqslant\Delta t\leqslant 3\cdot T_1$, that is, $-(6/2)T_1<\Delta t<(6/2)T_1$, only paths corresponding to values $|m|\leqslant 6$ can traverse the anti-Stokes lines. This is in agreement with Fig. 8 where indeed $z_{\pm 7}$ do not cross the anti-Stokes lines. Note that the paths $z_{\pm 6}$ are not present since $\mathcal{W}^{(2)}_{m=2k}=0$. Paths corresponding to values of m smaller than $m<-7$ have $|\arg[z_m(\Delta t)]|<\pi/3$ and hence yield vanishing values for the Airy function.

VI. UNIVERSAL SHAPE OF FRACTIONAL REVIVALS AND REVIVALS

By combining all properties of the constituents discussed in the preceding section we are now in a position to understand the location, the shape, and the fine structure of each fractional revival shown in Fig. 7(a). The multiplication of the Airy function by the exponential F_m and the Gaussian G results in a function, which has a pronounced peak in the vicinity of the time $\Delta t_m=(m/2)T_1$. Since the Gaussian varies slowly compared to the exponential and the Airy function, it only affects the height of this peak, but not its individual structure. This stands out most clearly in Fig. 7, where we show in (b) and (c) the function $I^{(2)}_m(\Delta t)$ together with the Gaussian $G(\Delta t)$, the exponential $F_m(\Delta t)$, and $|\mathrm{Ai}(z_m(\Delta t))|$ for $m=1$ and $m=5$, respectively. We note that the functions $I^{(2)}_{m=1}(\Delta t)$ and $I^{(2)}_{m=5}(\Delta t)$ reproduce the fractional revivals centered at $t=80.5T_1$ or $\Delta t=0.5T_1$ and $t=82.5T_1$ or $\Delta t=2.5T_1$, respectively. Hence we can identify each term $I^{(2)}_m$ in the sum Eq. (4.9) as a fractional revival labeled by the summation index m. In this case the terms $I^{(2)}_m$ in the sum Eq. (4.9) do not have significant overlap and we can approximate the absolute value of the sum in the immediate neighborhood of $\Delta t_m=(m/2)T_1$ by the mth term in the sum. Hence we find for $\Delta t\simeq\Delta t_m$

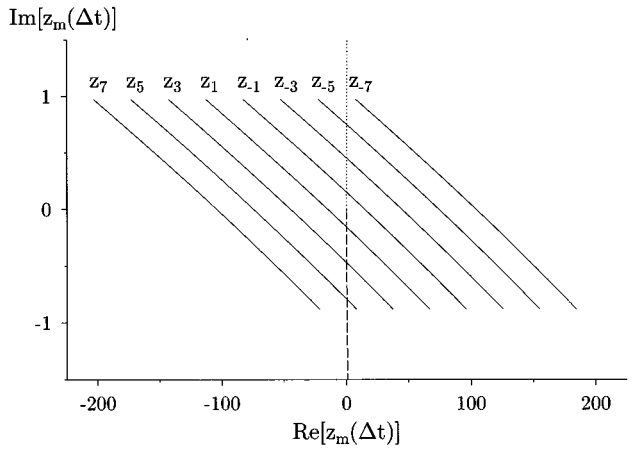

FIG. 8. The paths $z_m(\Delta t)$ in the complex plane governing the time dependence of the Airy function for the time interval $-3T_1<\Delta t<3T_1$ of Fig. 7. The paths correspond to $m=-7,-5,\ldots,5,7$. The two anti-Stokes lines $\arg(z)=\pm\pi/3$ (dotted and a dashed line) appear as a single vertical line due to the drastically different scales of the real and imaginary axes. During this time interval only the paths corresponding to $m=-5,\ldots,5$ cross these anti-Stokes lines. Note that the larger the absolute value of the index m, the larger the absolute value of the imaginary part of z_m when it crosses the anti-Stokes line.

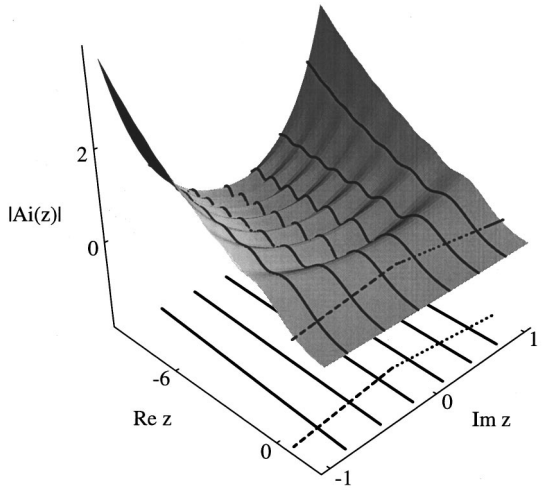

FIG. 9. The modulus $|\mathrm{Ai}(z)|$ of the Airy function of complex argument as a rolling valley above the complex plane. Thick lines in the complex plane represent the paths z_m for $m=-5,-3,\ldots,3,5$ starting with $m=-5$ in the back of the figure. Two of the anti-Stokes lines are depicted by dotted and dashed lines in accordance with Fig. 8. The values $|\mathrm{Ai}(z_m)|$ and $|\mathrm{Ai}(z=|z|e^{\pm i\pi/3})|$ of the Airy function along the paths z_m and along these anti-Stokes lines are indicated by thick lines. Note that this figure does not cover the entire excerpt of the complex plane shown in Fig. 8, but corresponds only to a thin vertical stripe in the vicinity of the anti-Stokes lines.

$$|S(\Delta t)|\cong|\mathcal{W}_m^{(2)}||I_m^{(2)}(\Delta t)|, \tag{6.1}$$

which with the help of Eq. (5.1) reads

$$|S(\Delta t)|\cong|\mathcal{W}_m^{(2)}|G(\Delta t)F_m(\Delta t)|\mathrm{Ai}(z_m(\Delta t))|. \tag{6.2}$$

Note that in this case the weight factor $\mathcal{W}_m^{(2)}$ takes on the values $|\mathcal{W}_{m=2k}^{(2)}|\equiv 0$ and $|\mathcal{W}_{m=2k+1}^{(2)}|\equiv 1$. Moreover, due to the separation of the individual terms only the absolute value of the Airy function enters and the phase factor $\exp[i\Phi_m(\Delta t)]$ has no influence on the modulus of S. This discussion clearly shows that the representation Eq. (4.9) of the sum S has the advantage that in an appropriate time domain $|\Delta t|$ around the fractional revival time $(q/r)T_2$ it allows a simple interpretation of the fractional revivals positioned in the neighborhood of $\Delta t_m=(m/r)T_1$: The mth term in the sum corresponds to the mth fractional revival. This identification, however, only works when the time Δt is in the immediate vicinity of the time $(q/r)T_2$. When $|\Delta t|$ becomes too large, consecutive terms in the sum overlap, interfere, and give rise to a complex structure. In this regime there is no simple one-to-one correspondence between individual terms of this representation and the signal pattern.

Before we discuss the conditions under which these terms separate, we first investigate the shape and the fine structure of the individual terms. From Fig. 7 we recognize that the striking oscillations on top of the slow decay to the left of the center of each fractional revival are a consequence of the oscillations of the Airy function [46]. We note that this oscillatory structure is also apparent in the measured fractional revivals of Ref. [17]. Comparing the fractional revival corresponding to $m=1$ to that of $m=5$ we find the latter to be broader with less pronounced oscillations. The sensitivity of the Airy function on the imaginary part of its argument as discussed in Fig. 9 explains this feature. To understand this we first recall that the oscillatory behavior of $I_m^{(r)}$ results from the temporal dependence of the argument $z_m(\Delta t)$ of the Airy function in the vicinity of the crossing time $\Delta t_m^{(a)}$. Figure 8 shows that a larger absolute value of the index m corresponds to a larger absolute value of the imaginary part of $z_m(\Delta t_m^{(a)})$. Since the Airy function increases dramatically with an increase of the imaginary part of its argument on the left domain of the anti-Stokes lines, that is, for $|\arg(z)|>\pi/3$, and loses at the same time in depth of its oscillations, the peak of the function $I_m^{(r)}(\Delta t)$ not only broadens for increasing values of $|m|$, but also shows less pronounced oscillations.

In the discussion of these oscillations the sign σ_3 of the cubic term in the expansion Eq. (2.2) plays a role. We note from Eqs. (A21) and (A25) that its value determines the side of the fractional revival on which the oscillatory pattern manifests itself: For $\sigma_3=+1$ this phenomenon occurs on the left hand side, whereas for $\sigma_3=-1$ it occurs on the right hand side [47]. In contrast, the value of σ_2 does not affect the shape of the signal. Indeed, Eq. (A21) shows that this quantity only determines the sign of the imaginary part of $z_m(\Delta t)$. When we recall the property $\mathrm{Ai}(z^\star)=\mathrm{Ai}^\star(z)$ following from the definition of the Airy function, Eq. (A12), we realize that a conjugation of its complex argument does not change the modulus of the Airy function.

We now address the conditions under which neighboring functions $I_m^{(r)}$ with nonvanishing weights $\mathcal{W}_m^{(r)}$ separate. They separate, if their widths $\delta t_m^{(r)}$ are smaller than the distance δt_r between their dominant peaks located in the neighborhood of the crossing time $\Delta t_m^{(a)}\simeq\Delta t_m=(m/r)T_1$, that is, $\delta t_m^{(r)}<\delta t_r$. Note that the separation δt_r depends neither on

the index m nor on the time Δt, but is only a function of r: Due to the properties of the weight factor $\mathcal{W}_m^{(r)}$ it is given by $\delta t_r=(1/r)T_1$ for r odd and $\delta t_r=(2/r)T_1$ for r even. Thus this separation is completely determined by the choice of the fraction q/r in Eq. (4.1). On the other hand, the width $\delta t_m^{(r)}$ of the function $I_m^{(r)}(\Delta t)$ depends on the index m: As shown in Figs. 7(b) and 7(c) a larger value of $|m|$ results in a broader fractional revival. Hence neighboring nonvanishing terms in Eq. (4.9) inevitably overlap as $|m|$ exceeds a certain value. If two functions $I_m^{(r)}(\Delta t)$ and $I_{m'}^{(r)}(\Delta t)$ overlap considerably, interferences between these terms in Eq. (4.9) arise. Then the function $\exp[i\Phi_m(\Delta t)]$ and the phase of the complex Airy function start to play an important role. Consequently, the sum S exhibits a more complicated pattern. This is apparent in Figs. 5(a) and 7(b) from the behavior of the sum $|S(t)|$ at the edges of the time intervals.

We note, however, that for even larger times, we can analyze the structures again by noting that larger values of $|\Delta t|$ correspond to a different time regime and a new characterization $(q/r)T_2$ in Eq. (4.1): A new choice of the fraction q/r enables us to separate again neighboring peaks, since the separation δt_r of the peaks is only a function of r, whereas the widths of the peaks $\delta t_m^{(r)}$ depend via m on Δt.

VII. SUMMARY

In this paper we investigate in detail the time dependence of typical transient signals encountered in many different fields of physics and chemistry. Instead of focusing on a specific system, we adopt a rather general point of view and study a generic signal, which consists of a coherent sum of many harmonics whose phases depend nonlinearly on the summation index. Signals of this kind exhibit interesting phenomena such as quasiperiodic evolution, dephasing, fractional revivals, and full revivals. These features are the result of interference between many contributing states. In this paper we present analytical expressions for such signals in different time regimes.

The key to the deeper understanding of the phenomena springs from a new representation of this sum. However, there exist many equivalent representations of such signals. Most convenient, to understand the time dependence of the signal in a specific time region of interest, is the one which represents it as a sequence of signals separated in time. In the short-time limit, that is, for $t \ll T_2$, the application of the Poisson summation formula is enough to achieve such a new representation. However, for times of the order of T_2 a more complicated transformation of the initial sum is necessary. The resulting new representation enables us to provide closed-form expressions for each single peak of the signal as in the short time limit. These expressions depend on parameters, which are determined by the specific physical system and the time interval of interest.

Our approach allows us to understand even the fine details of each individual peak of a transient signal. We find that the peaks in the pattern in the early stage of the evolution are symmetric. In contrast, the fractional revivals and full revivals have asymmetric shapes depending on the parameters of the system: On one side of their center they may show an oscillatory behavior. This behavior stems from an Airy function of complex argument which results from the cubic term in the expansion Eq. (2.2) of the relevant frequencies of the system. Whether the Airy function manifests itself in the shape of the fractional revivals and full revivals depends on the specific parameters such as the time scale T_3 and the width Δn of the distribution P_n [48]. The sign σ_3 of the third derivative of the frequencies $\omega(n)$ with respect to the parameter n determines on which side of the center the oscillations occur. In contrast, the sign of σ_2 does not affect the shape of the signal. We also note that each individual fractional revival in a group may differ from its immediate neighbor, although overall features such as their mutual distances are the same within one group.

We conclude by emphasizing that due to the generality of our approach this method can describe many phenomena in atomic and molecular physics as well as quantum optics.

ACKNOWLEDGMENTS

We thank M. Shapiro and D. Abrashkevich for providing the data for the autocorrelation function shown in Fig. 2. We acknowledge valuable discussions with V. M. Akulin in the early stage of this work and thank him for a critical reading of the final manuscript. We are grateful to M. V. Berry for his stimulating comments and for sending us his work on this topic prior to publication. One of us (I.A.) appreciates the kind hospitality and support at the Universität Ulm. C.L. thanks the Deutsche Forschungsgemeinschaft for its support and acknowledges the warm hospitality during his stay at the Weizmann Institute of Science, Rehovot.

APPENDIX A: EVALUATION OF THE INTEGRAL EQ. (4.11)

In this appendix, we evaluate the integral

$$I_m^{(r)}(\Delta t)=\int_{-\infty}^{\infty} dx P(\overline{n+}x)\exp\left\{2\pi i\left[\left(\frac{\Delta t}{T_1}-\frac{m}{r}\right)x+\sigma_2\left(\epsilon_{q/r}+\frac{\Delta t}{T_1}\right)\frac{T_1}{T_2}x^2+\sigma_3\left(l+\frac{\Delta t}{T_1}\right)\frac{T_1}{T_3}x^3\right]\right\} \tag{A1}$$

for the example of a Gaussian distribution

$$P(\overline{n+}x)=\frac{1}{\sqrt{2\pi\Delta n^2}}\exp\left(-\frac{x^2}{2\Delta n^2}\right). \tag{A2}$$

For this purpose it is of advantage to have a positive coefficient in front of x^3 in the exponent in $I_m^{(r)}$. We therefore introduce the new integration variable $y=\sigma_3 x$ which yields

$$I_m^{(r)}(\Delta t)=\int_{-\infty}^{\infty} dy P(\overline{n+}y)\exp\left\{2\pi i\left[\sigma_3\left(\frac{\Delta t}{T_1}-\frac{m}{r}\right)y+\sigma_2\left(\epsilon_{q/r}+\frac{\Delta t}{T_1}\right)\frac{T_1}{T_2}y^2+\left(l+\frac{\Delta t}{T_1}\right)\frac{T_1}{T_3}y^3\right]\right\}. \tag{A3}$$

Note that this substitution leaves the terms quadratic in x

invariant, but does change the terms linear and cubic in x. Moreover, the limits of integration are unchanged.

Hence the integral $I_m^{(r)}$ is of the form

$$J=\int_{-\infty}^{\infty} dy \exp[i(\alpha y+\beta y^2+\delta y^3)], \tag{A4}$$

where

$$\alpha \equiv 2\pi\sigma_3\left(\frac{\Delta t}{T_1}-\frac{m}{r}\right) \tag{A5}$$

and

$$\delta \equiv 2\pi\left(l+\frac{\Delta t}{T_1}\right)\frac{T_1}{T_3}>0 \tag{A6}$$

are real-valued parameters, whereas the parameter

$$\beta \equiv \beta_R+i\beta_I=2\pi\sigma_2\left(\epsilon_{q/r}+\frac{\Delta t}{T_1}\right)\frac{T_1}{T_2}+i\frac{1}{2\Delta n^2} \tag{A7}$$

becomes complex. Since $\delta>0$ we can substitute

$$y \equiv \left(\frac{1}{3\delta}\right)^{1/3} x-\frac{\beta}{3\delta}, \tag{A8}$$

which eliminates the term quadratic in the integration variable y via the relation

$$\begin{aligned}\alpha y+\beta y^2+\delta y^3 &= \frac{x^3}{3}+\left(\frac{1}{3\delta}\right)^{1/3}\left(\alpha-\frac{\beta^2}{3\delta}\right)x+\frac{2\beta^3}{27\delta^2}-\frac{\alpha\beta}{3\delta} \\ &\equiv \frac{x^3}{3}+zx+\kappa,\end{aligned} \tag{A9}$$

where

$$z \equiv \left(\frac{1}{3\delta}\right)^{1/3}\left(\alpha-\frac{\beta^2}{3\delta}\right) \tag{A10}$$

and

$$\kappa \equiv \frac{2\beta^3}{27\delta^2}-\frac{\alpha\beta}{3\delta}. \tag{A11}$$

This transformation allows us to express the integral J in a product consisting of an Airy function

$$\mathrm{Ai}(z)=\frac{1}{2\pi}\int_{-\infty}^{\infty} dx\ \exp\left[i\left(\frac{x^3}{3}+zx\right)\right] \tag{A12}$$

of complex argument z, and a complex-valued exponential. Indeed we find from Eq. (A4) using Eqs. (A8), (A9), and (A12)

$$J=\frac{2\pi}{(3\delta)^{1/3}}\exp(i\kappa)\mathrm{Ai}(z). \tag{A13}$$

Since β is a complex number it is of advantage to express z and κ in their real and imaginary part. The relations

$$\beta^2=\beta_R^2-\beta_I^2+i2\beta_R\beta_I \tag{A14}$$

and

$$\beta^3=\beta_R^3-3\beta_R\beta_I^2+i(3\beta_R^2\beta_I-\beta_I^3) \tag{A15}$$

yield

$$z=\left(\frac{1}{3\delta}\right)^{1/3}\left(\alpha-\frac{\beta_R^2-\beta_I^2}{3\delta}\right)-i\left(\frac{1}{3\delta}\right)^{1/3}\frac{2\beta_R\beta_I}{3\delta} \tag{A16}$$

and

$$\begin{aligned}\kappa \equiv \kappa_R+i\kappa_I &= \frac{2}{27\delta^2}(\beta_R^3-3\beta_R\beta_I^2)-\frac{\alpha\beta_R}{3\delta} \\ &+i\left[\frac{2}{27\delta^2}(3\beta_R^2\beta_I-\beta_I^3)-\frac{\alpha\beta_I}{3\delta}\right].\end{aligned} \tag{A17}$$

Using these abbreviations and the result Eq. (A13) for J, the integral $I_m^{(r)}$ Eq. (A3) with $P(n)$ given by Eq. (A2) reads

$$I_m^{(r)}(\Delta t)=\frac{\sqrt{2\pi}}{\Delta n(3\delta)^{1/3}}\exp(-\kappa_I)\exp(i\kappa_R)\mathrm{Ai}(z). \tag{A18}$$

We conclude by substituting the expressions for α, δ, and β, that is, Eqs. (A5), (A6), and (A7) into Eqs. (A16) and (A17) and arrive at

$$\begin{aligned}\kappa_R \equiv \Phi_m(\Delta t) &= \frac{4\pi}{27}\sigma_2\left(\epsilon_{q/r}+\frac{\Delta t}{T_1}\right)\frac{T_1}{T_2}\left[\frac{T_3}{2\pi(lT_1+\Delta t)}\right]^2 \\ &\times\left\{\left[2\pi\left(\epsilon_{q/r}+\frac{\Delta t}{T_1}\right)\frac{T_1}{T_2}\right]^2-\frac{3}{4\Delta n^4}\right\} \\ &-\frac{4\pi^2}{3}\sigma_2\sigma_3\left(\epsilon_{q/r}+\frac{\Delta t}{T_1}\right)\frac{T_1}{T_2}\left(\frac{\Delta t}{T_1}-\frac{m}{r}\right)\frac{T_3}{2\pi(lT_1+\Delta t)}\end{aligned} \tag{A19}$$

and

$$\begin{aligned}\kappa_I &= \left[\frac{T_3}{3\Delta n(lT_1+\Delta t)}\right]^2\left[\left(\epsilon_{q/r}+\frac{\Delta t}{T_1}\right)^2\left(\frac{T_1}{T_2}\right)^2-\frac{1}{48\pi^2\Delta n^4}\right] \\ &-\frac{\sigma_3 T_3}{6\Delta n^2(lT_1+\Delta t)}\left(\frac{\Delta t}{T_1}-\frac{m}{r}\right)\end{aligned} \tag{A20}$$

together with

$$
\begin{aligned}
z &\equiv z_m(\Delta t) \\
&= \left[\frac{T_3}{6\pi(lT_1+\Delta t)}\right]^{1/3} 2\pi\sigma_3\left(\frac{\Delta t}{T_1}-\frac{m}{r}\right) \\
&\quad -\left[\frac{T_3}{6\pi(lT_1+\Delta t)}\right]^{4/3}\left[4\pi^2\left(\epsilon_{q/r}+\frac{\Delta t}{T_1}\right)^2\left(\frac{T_1}{T_2}\right)^2-\frac{1}{4\Delta n^4}\right] \\
&\quad -i\left[\frac{T_3}{6\pi(lT_1+\Delta t)}\right]^{4/3}\frac{2\pi\sigma_2}{\Delta n^2}\left(\epsilon_{q/r}+\frac{\Delta t}{T_1}\right)\frac{T_1}{T_2}. \qquad \text{(A21)}
\end{aligned}
$$

With these expressions we find from Eq. (A18)

$$
\begin{aligned}
I_m^{(r)}(\Delta t) &= A\exp[i\Phi_m(\Delta t)]\exp\left[-\lambda\left(\epsilon_{q/r}+\frac{\Delta t}{T_1}\right)^2\right] \\
&\quad \times\exp\left[\mu\left(\frac{\Delta t}{T_1}-\frac{m}{r}\right)\right]\mathrm{Ai}[z_m(\Delta t)], \qquad \text{(A22)}
\end{aligned}
$$

where the quantities

$$
\begin{aligned}
A &= A(\Delta t) \\
&\equiv \frac{\sqrt{2\pi}}{\Delta n}\left[\frac{T_3}{6\pi(lT_1+\Delta t)}\right]^{1/3}\exp\left[\frac{1}{3}\left(\frac{T_3}{12\pi\Delta n^3(lT_1+\Delta t)}\right)^2\right], \qquad \text{(A23)}
\end{aligned}
$$

and

$$
\lambda = \lambda(\Delta t) \equiv \left[\frac{T_1T_3}{3\Delta n(lT_1+\Delta t)T_2}\right]^2 \qquad \text{(A24)}
$$

and

$$
\mu = \mu(\Delta t) \equiv \frac{\sigma_3 T_3}{6\Delta n^2(lT_1+\Delta t)} \qquad \text{(A25)}
$$

are functions of Δt.

So far the calculation is exact. We note that in general the time dependence of $I_m^{(r)}(\Delta t)$ originates from the time dependence of the phase $\Phi_m(\Delta t)$, the Gaussian, the exponential, and the Airy function as well as from the time dependence of the quantities $A(\Delta t)$, $\lambda(\Delta t)$, and $\mu(\Delta t)$. However, for the parameters used in this paper, this time dependence simplifies considerably: In the vicinity $|\Delta t| \sim T_1$ of a fractional revival time $t = q/rT_2 \simeq lT_1$ where $l \gg 1$, we can replace $lT_1+\Delta t \simeq lT_1 \pm T_1 \simeq lT_1$, that is, we can neglect the time dependence of A, λ and μ and evaluate these quantities at $\Delta t = 0$.

APPENDIX B: CROSSING AN ANTI-STOKES LINE

In this appendix we determine the time $\Delta t_m^{(a)}$ at which the path $z_m(\Delta t)$ crosses an anti-Stokes line $\arg(z) = \pm\pi/3$. This time follows from the equation

$$
\tan\{\arg[z_m(\Delta t_m^{(a)})]\} = \frac{\mathrm{Im}[z_m(\Delta t_m^{(a)})]}{\mathrm{Re}[z_m(\Delta t_m^{(a)})]} = \tan\left(s\frac{\pi}{3}\right) = s\sqrt{3}. \qquad \text{(B1)}
$$

Here, $s = \pm 1$ corresponds to the anti-Stokes line $\arg(z) = \pi/3$ and $\arg(z) = -\pi/3$, respectively. Note that the real part of z_m must be positive and $s = \pm 1$ corresponds to a positive and negative imaginary part of z_m, respectively. When we insert the real and imaginary parts of Eq. (A21) into Eq. (B1), we arrive at the quadratic equation for $\Delta t_m^{(a)}$

$$
a\left(\frac{\Delta t_m^{(a)}}{T_1}\right)^2 + b\frac{\Delta t_m^{(a)}}{T_1} + c = 0, \qquad \text{(B2)}
$$

where the quantities a, b, and c are defined by

$$
a \equiv 6\pi\sigma_3\frac{T_1}{T_3} - 2\pi\left(\frac{T_1}{T_2}\right)^2, \qquad \text{(B3)}
$$

and

$$
b \equiv 6\pi\sigma_3\left(l-\frac{m}{r}\right)\frac{T_1}{T_3} - 4\pi\epsilon_{q/r}\left(\frac{T_1}{T_2}\right)^2 + s\sigma_2\frac{1}{\sqrt{3}\Delta n^2}\frac{T_1}{T_2}, \qquad \text{(B4)}
$$

and

$$
c \equiv \frac{1}{8\pi\Delta n^4} + s\sigma_2\frac{\epsilon_{q/r}}{\sqrt{3}\Delta n^2}\frac{T_1}{T_2} - 6\pi l\frac{m}{r}\frac{T_1}{T_3} - 2\pi\epsilon_{q/r}^2\left(\frac{T_1}{T_2}\right)^2. \qquad \text{(B5)}
$$

Now we turn to our specific example, Fig. 7. For the parameters we use in this figure we find $|4ac/b^2| \ll 1$. In this case $\Delta t_m^{(a)}$ can be well approximated by $\Delta t_m^{(a)} \simeq -(c/b)T_1$, and the parameters b and c now read

$$
b = 6\pi\left(l-\frac{m}{2}\right)\frac{T_1}{T_3} + s\frac{1}{\sqrt{3}\Delta n^2}\frac{T_1}{T_2}, \qquad \text{(B6)}
$$

and

$$
c = \frac{1}{8\pi\Delta n^4} - 6\pi l\frac{m}{2}\frac{T_1}{T_3}, \qquad \text{(B7)}
$$

since $\epsilon_{1/2} = 0$ for the example at hand. Moreover, for $|m| < 7$ corresponding to Fig. 9, the parameters b and c can be further simplified to $b \simeq 6\pi lT_1/T_3$ and $c \simeq -6\pi lmT_1/(2T_3)$. Hence in this case the time point $\Delta t_m^{(a)}$ is given by

$$
\Delta t_m^{(a)} \simeq -\frac{c}{b}T_1 \simeq \frac{m}{2}T_1, \qquad \text{(B8)}
$$

that is, the path $z_m(\Delta t)$ crosses an anti-Stokes line in the immediate vicinity of $\Delta t_m = (m/2)T_1$.

[1] Over the last few years numerous papers about this subject appeared, mainly in atomic physics and molecular physics. For a review of electronic wave packets in Rydberg atoms, see, e.g., G. Alber and P. Zoller, Phys. Rep. **199**, 231 (1990). For a review of vibrational wave packets in molecular physics see, e.g., M. Gruebele and A. Zewail, Phys. Today **43**, 24 (1990); B. Garraway, S. Stenholm, and K.-A. Suominen, Phys. World **6**, 46 (1993); and B. Garraway and K.-A. Suominen, Rep.

Prog. Phys. **58**, 365 (1995). General aspects of the dynamics of wave packets in atomic, molecular, and quantum optical systems are discussed in a review article by I. Sh. Averbukh and N. F. Perel'man, Usp. Fiz. Nauk **161**, 41 (1991) [Sov. Phys. Usp. **34**, 572 (1991)].

[2] M. Nauenberg, C. R. Stroud, Jr., and J. Yeazell, Sci. Am. **270**, 24 (1994).

[3] A. H. Zewail, *Femtochemistry* (World Scientific, Singapore, 1994), Vols. 1 and 2.

[4] J. Manz and L. Wöste, *Femtosecond Chemistry* (VCH, Weinheim, 1995), Vols. 1 and 2.

[5] J. Parker and C. R. Stroud, Jr., Phys. Rev. Lett. **56**, 716 (1986).

[6] G. Alber, H. Ritsch, and P. Zoller, Phys. Rev. A **34**, 1058 (1986); G. Alber and P. Zoller, *ibid.* **37**, 337 (1988).

[7] M. Nauenberg, Phys. Rev. A **40**, 1139 (1989); Comments At. Mol. Phys. **25**, 151 (1990); J. Phys. B **23**, L385 (1990).

[8] Z. Dačić Gaeta and C. R. Stroud, Jr., Phys. Rev. A **42**, 6308 (1990).

[9] A. Peres, Phys. Rev. A **47**, 5196 (1993).

[10] S. D. Boris, S. Brandt, H. D. Dahmen, T. Stroh, and M. L. Larsen, Phys. Rev. A **48**, 2574 (1993).

[11] A semiclassical treatment of fractional revivals and full revivals based on the use of multiple reference trajectories is given in I. M. Suarez Barnes, M. Nauenberg, M. Nockleby, and S. Tomsovic, Phys. Rev. Lett. **71**, 1961 (1993), whereas the approach by M. Mallalieu and C. R. Stroud, Jr., Phys. Rev. A **51**, 1827 (1995) is based on the classical-path representation.

[12] R. Bluhm and V. A. Kostelecký, Phys. Rev. A **49**, 4628 (1994); **50**, R4445 (1994); **51**, 4767 (1995).

[13] P. A. Braun and V. I. Savichev, Phys. Rev. A **49**, 1704 (1994).

[14] A. ten Wolde, L. D. Noordam, H. G. Muller, and H. B. van Linden van den Heuvell, in *Fundamentals of Laser Interactions*, edited by F. Ehlotzky (Springer-Verlag, Heidelberg, 1989).

[15] J. A. Yeazell, M. Mallalieu, and C. R. Stroud, Jr., Phys. Rev. Lett. **64**, 2007 (1990); J. A. Yeazell and C. R. Stroud, Jr., Phys. Rev. A **43**, 5153 (1991).

[16] D. R. Meacher, P. E. Meyler, I. G. Hughes, and P. Ewart, J. Phys. B **24**, L63 (1991).

[17] J. Wals, H. H. Fielding, J. F. Christian, L. C. Snoek, W. J. van der Zande, and H. B. van Linden van den Heuvell, Phys. Rev. Lett. **72**, 3783 (1994); J. Wals, H. H. Fielding, and H. B. van Linden van den Heuvell, Phys. Scr. **T58**, 62 (1995).

[18] L. Marmet, H. Held, G. Raithel, J. A. Yeazell, and H. Walther, Phys. Rev. Lett. **72**, 3779 (1994); G. Raithel, H. Held, L. Marmet, and H. Walther, J. Phys. B **27**, 2849 (1994).

[19] For the use of fractional revivals to demonstrate the self-interference of an electron, see M. Noel and C. R. Stroud, Jr., Phys. Rev. Lett. **75**, 1252 (1995).

[20] M. Gruebele and A. H. Zewail, J. Chem. Phys. **98**, 883 (1993).

[21] Ch. Meier, V. Engel, and J. S. Briggs, J. Chem. Phys. **95**, 7337 (1991); Ch. Meier and V. Engel, Chem Phys. Lett. **212**, 691 (1993).

[22] S. I. Vetchinkin, A. S. Vetchinkin, V. V. Eryomin, and I. M. Umanskii, Chem. Phys. Lett. **215**, 11 (1993); S. I. Vetchinkin and V. V. Eryomin, *ibid.* **222**, 394 (1994).

[23] T. Baumert, V. Engel, C. R. Röttgermann, W. T. Strunz, and G. Gerber, Chem. Phys. Lett. **191**, 639 (1992); T. Baumert and G. Gerber, Isr. J. Chem. **34**, 103 (1994).

[24] I. Fischer, D. M. Villeneuve, M. J. J. Vrakking, and A. Stolow, J. Chem. Phys. **102**, 5566 (1995); M. J. J. Vrakking, D. M. Villeneuve, and A. Stolow, Phys. Rev. A **54**, R37 (1996).

[25] For the revivals in the Jaynes-Cummings model, see, for example, J. H. Eberly, N. B. Narozhny, and J. J. Sanchez-Mondragon, Phys. Rev. Lett. **44**, 1323 (1980); N. B. Narozhny, J. J. Sanchez-Mondragon, and J. H. Eberly, Phys. Rev. A **23**, 236 (1981); H. I. Yoo and J. H. Eberly, Phys. Rep. **118**, 239 (1985).

[26] B. Yurke and D. Stoler, Phys. Rev. Lett. **57**, 13 (1986); Physica B **151**, 298 (1988).

[27] A. Miranowicz, R. Tanás, and S. Kielich, Quantum Opt. **2**, 253 (1990).

[28] J. Eiselt and H. Risken, Phys. Rev. A **43**, 346 (1991).

[29] I. Sh. Averbukh, Phys. Rev. A **46**, R2205 (1992).

[30] M. Fleischhauer and W. P. Schleich, Phys. Rev. A **47**, 4258 (1993).

[31] P. F. Gorá and C. Jedrzejek, Phys. Rev. A **48**, 3291 (1993); **49**, 3046 (1994).

[32] G. Rempe, H. Walther, and N. Klein, Phys. Rev. Lett. **58**, 353 (1987).

[33] M. Brune, F. Schmidt-Kaler, A. Maali, J. Dreyer, E. Hagley, J.M. Raimond, and S. Haroche, Phys. Rev. Lett. **76**, 1800 (1996).

[34] For the phenomenon of Jaynes-Cummings revivals in the quantum motion of ions in a Paul trap, see C. A. Blockley, D. F. Walls, and H. Risken, Europhys. Lett. **17**, 509 (1992); J. I. Cirac, R. Blatt, A. S. Parkins, and P. Zoller, Phys. Rev. A **49**, 1202 (1994); W. Vogel and R. L. de Matos Filho, *ibid.* **52**, 4214 (1995).

[35] The Jaynes-Cummings revivals in the Paul trap have been observed experimentally by D. M. Meekhof, C. Monroe, B. E. King, W. M. Itano, and D. J. Wineland, Phys. Rev. Lett. **76**, 1796 (1996).

[36] In the context of classical optics, a similar phenomenon is known as the Talbot effect: Here, it represents the self-imaging of a grating, which is illuminated by plane waves, in the near field. This effect was first observed by H. F. Talbot, Philos. Mag. **9**, 401 (1836), and explained much later by L. Rayleigh, *ibid.* **11**, 196 (1881). Just recently, this effect was also demonstrated for atomic waves; see M. S. Chapman, C. S. Ekstrom, T. D. Hammond, J. Schmiedmayer, B. E. Tannian, S. Wehinger, and D. E. Pritchard, Phys. Rev. A **51**, R14 (1995).

[37] S. Dyrting and G. J. Milburn, Phys. Rev. A **47**, R2484 (1993); W.-Y. Chen and G. J. Milburn, *ibid.* **51**, 2328 (1995).

[38] Note, however, that the Jaynes-Cummings revivals discussed and observed in Refs. [25,30,32–35] correspond to the classical oscillation of an atomic or molecular wave packet between the turning points. They occur in the early stage of the evolution at integer multiples of T_1. For the discussion of fractional revivals and full revivals in the Jaynes-Cummings model analogous to the ones in atoms and molecules, that is, at fractions of T_2, see, for example, Ref. [29]. However, these long-time phenomena have not yet been observed experimentally in the Jaynes-Cummings model.

[39] Actually, we find already a recurrence of the initial periodic behavior, that is, a sequence of peaks with period T_1, after the time $T_2/2$. However, as we will see later, this pattern is shifted by half of the period T_1 with respect to the initial structure [40]. Despite this, some authors refer to $T_2/2$ as the revival time.

[40] I. Sh. Averbukh and N. F. Perel'man, Phys. Lett. A **139**, 449

(1989); Zh. Éksp. Teor. Fiz. **96**, 818 (1989) [Sov. Phys. JETP **69**, 464 (1989)].

[41] In fact, this is the most discussed case in the literature, since in pump-probe experiments the exciting laser pulse often has a Gaussian shape, which yields a Gaussian or near Gaussian weight function P_n. However, the typical features of transient signals do not change significantly for non-Gaussian weights, as long as P_n is centered about some dominant maximum with a width $\Delta n \gg 1$.

[42] This method was already employed successfully by different authors; see, e.g., [6,7,30].

[43] R. Courant and D. Hilbert, *Methods of Mathematical Physics* (Interscience Publishers, New York, 1953).

[44] For a similar technique to treat the integral, fractional, and fractal Talbot effect, see M. V. Berry (unpublished) and M. V. Berry and S. Klein (unpublished).

[45] Here we follow the definition of M. V. Berry and K. E. Mount, Rep. Prog. Phys. **35**, 315 (1972) or J. Heading, *An Introduction to Phase Integral Methods* (Methuen, London, 1962). In contrast, C. M. Bender and S. A. Orszag, *Advanced Mathematical Methods for Scientists and Engineers* (McGraw-Hill, Singapore, 1984), p. 116 refer to the anti-Stokes lines defined by $\arg(z) = \pm \pi/3$ and $\arg(z) = \pi$ as Stokes lines.

[46] Several authors [8,10,12,17] have mentioned the effect of the cubic term in the sum Eq. (2.4). However, no closed-form expressions for the shape of fractional revivals and revivals were given. For example, Ref. [17] pointed out that in their measured autocorrelation function ''a small forerunner wave packet'' precedes the main wave packet for $t \simeq T_2/2$. This small forerunner represents the first oscillation due to the Airy function as shown in this paper. We can therefore interpret this forerunner as ''rainbow scattering in the time domain;'' see, for example, the article by M. V. Berry and K. E. Mount, Ref. [45].

[47] In the case of Rydberg atoms with eigenfrequencies $\omega(n) \propto -1/n^2$ as well as in the Jaynes-Cummings model with Rabi frequencies $\omega(n) \propto \sqrt{n}$ we have $\sigma_3 = +1$.

[48] In some examples, such as the example of a vibrational wave packet propagating in the excited potential surface $A^1\Sigma_u^+$ of the sodium dimer shown in Fig. 2, the time scale T_3 does not significantly affect the shape of the signal for times of the order T_2, since here T_3 is very large compared to T_2. Two prominent examples, where this is *exactly* true for *all* times, are the Morse potential and a box with infinitely steep and infinitely high walls. For these systems, the third derivative and all higher derivatives of the eigenfrequencies $\omega(n)$ with respect to the quantum number n vanish. In this case, the fractional revivals and full revivals do not exhibit an oscillatory behavior, but have the same shape as in the initial stage of the evolution.

[49] For the prediction of higher-order (fractional) revivals beyond the time scale T_2, see O. Knospe and R. Schmidt, Phys. Rev. A **54**, 1154 (1996).